Journal of Physics: Conference Series **440** (2013) 012013 doi:10.1088/1742-6596/440/1/012013

Observational consequences of the local re-acceleration thick-target model

M Varady[1], Z Moravec[1], M Karlický[2], J Kašparová[2]

[1]Faculty of Science, J.E. Purkyně University, Physics Department, České mládeže 8, 400 75 Ústí nad Labem, Czech Republic

[2]Astronomical Institute of the Academy of Sciences of the Czech Republic, v.v.i., 251 65 Ondřejov , Czech Republic

E-mail: mvarady@physics.ujep.cz

Abstract. In our contribution we compare the efficiency of the hard X-ray production and the vertical sizes and positions of the hard X-ray sources for the classical collisional thick-target model and for its recently proposed modification, the local re-acceleration thick-target model. The latter model has been proposed in order to ease some of the severe theoretical problems of the collisional thick-target model related to interpretation of the observational properties of the foot-point HXR sources in solar flares. The results are obtained using a relativistic test-particle approach for a fully ionised atmosphere with a converging magnetic field and a single (compact) flare loop.

1. Introduction

The Collisional Thick-Target Model (CTTM) of the impulsive phase of solar flares [1] presented for many years a quite successful tool to interpret the fundamental processes related to the energy deposition and hard X-ray (HXR) production at the foot-point regions of flare loops due to the interaction of chromospheric plasma with electron beams. On the other hand, in order to explain the energetics of flares and observed intensities of HXR, many serious theoretical problems emerged (see [2] and the Introduction in [3]), especially in combination with the idea that the beam acceleration site corresponds to the coronal reconnection site [4], [5], [6] and consequently with the inevitability to transport enormous fluxes of accelerated charged particles from the corona to the thick-target region. Moreover novel RHESSI measurements of HXR chromospheric albedo [7] or of the vertical sizes and positions of the HXR sources are inconsistent with the predictions given by the CTTM [8], [9].

To resolve the discrepancies a modification of the CTTM known as the Local Re-acceleration Thick-Target Model (LRTTM) has recently been proposed [3], [10], [11]. The model assumes an existence of a secondary re-acceleration region located within the thick-target region in the chromosphere. The non-thermal electrons initially accelerated at the primary coronal acceleration site experience, in addition to the energy losses and scattering due to the Coulomb collisions, also sequences of re-acceleration events at the secondary re-acceleration region due to the stochastic electric fields generated in the current sheet cascades [10], [11] excited by random photospheric motions.

In our contribution we concentrate on a comparison of outcomes of the chromospheric bombardment by electron beams with a power-law spectrum modelled in frame of the CTTM

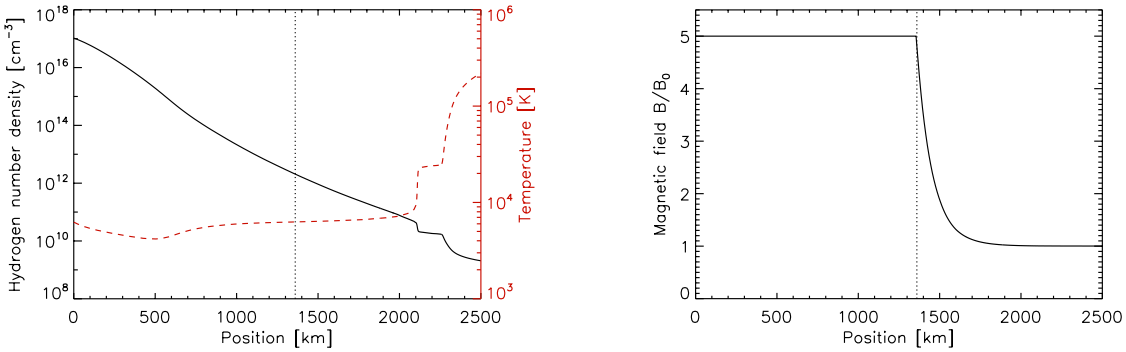

Figure 1. Left: Density (black solid line) and temperature (red dashed line) profiles of the VAL C atmosphere [12]. The dotted line indicates the bottom boundary of the magnetic mirror. Right: Relative magnetic field strength along the loop. Only the lower part of the atmosphere is plotted.

and LRTTM. We compare the non-thermal electron distribution functions in the vicinity of the thick-target region, corresponding chromospheric energy deposits, HXR production, spectra and vertical sizes and heights above the photosphere (corresponding to $\tau = 1$ at 5000 Å) of the HXR foot-point sources calculated for a fully ionised VAL C atmosphere [12] and a single (compact) loop with a converging magnetic field towards the photosphere. The results are obtained using a relativistic test-particle code [13], [14], [15].

2. Model description

The starting point of our simulations is a generation of an electron beam with a power-law spectrum and with parameters: power-law index $\delta = 3$, low-energy cutoff $E_0 = 10$ keV, high-energy cutoff $E_1 = 400$ keV, initial energy flux $\mathcal{F}_0 = 2.5 \times 10^9$ erg cm^{-2} s^{-1} (or 5×10^{10} erg cm^{-2} s^{-1} – the reference flux for the CTTM) and a normalised semi-uniform initial distribution of the pitch angle cosine $\mu_0 = \cos\vartheta \in (0.5, 1)$. In order to demonstrate the potential of secondary re-acceleration we selected a very small value of $\mathcal{F}_0$ in context of flare physics. As the target atmosphere in the presented approximation is static, by changing $\mathcal{F}_0$ the vertical structure of the distribution function remains the same and the energy deposits and HXR intensities scale linearly. In our model we assume that the beam is accelerated at the primary acceleration site localised in the corona. Using a relativistic test-particle code [13], [14], [15], we model the propagation of beam electrons through a fully ionised, static atmosphere with a converging magnetic field with the mirror ratio $R_m = 5$ (see right panel of Fig. 1). The temperature and density profiles of the atmosphere correspond to the VAL C model [12] (see left panel of Fig. 1) with an extension into the corona, the ionisation is artificially set to one in the whole atmosphere. The code calculates the corresponding Coulomb collisional energy losses and scattering and the effects of the magnetic mirroring in the converging field for the CTTM. For the LRTTM it also includes the effects of the secondary re-acceleration events due to the presence of the stochastic electric fields in the vicinity of the thick-target region. Only one-half of the loop is considered.

We assume normally distributed stochastic electric fields in the directions parallel and antiparallel relative to the loop axis, i.e. a simplified model of the electric field distribution due to the current sheet cascade in a randomly stressed magnetic loop in the chromosphere [3], [11]. We present results for zero mean value of the stochastic field and for its variances var$(E) = 0.5, 1$ and 5 V m^{-1}. The secondary re-acceleration region is placed into the chromosphere in range of

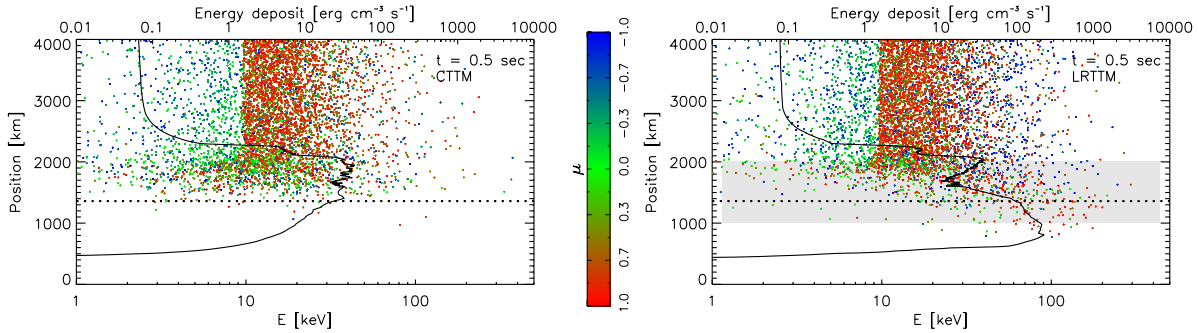

Figure 2. The distribution functions of non-thermal electron energies versus positions with a colour coded μ-distribution for the classical the CTTM (left panel) and LRTTM (right panel) for $\mathrm{var}(E) = 1$ V m^{-1} at time $t = 0.5$ s after the beam injection into the loop at its apex. The solid lines indicate the instantaneous energy deposit corresponding to $\mathcal{F}_0 = 2.5 \times 10^9$ erg cm^{-3} s^{-1} in the logarithmic scale. The dotted horizontal line indicates the bottom boundary of the magnetic mirror, the grey area corresponds the secondary re-acceleration region. Only the lower parts of the loop are captured.

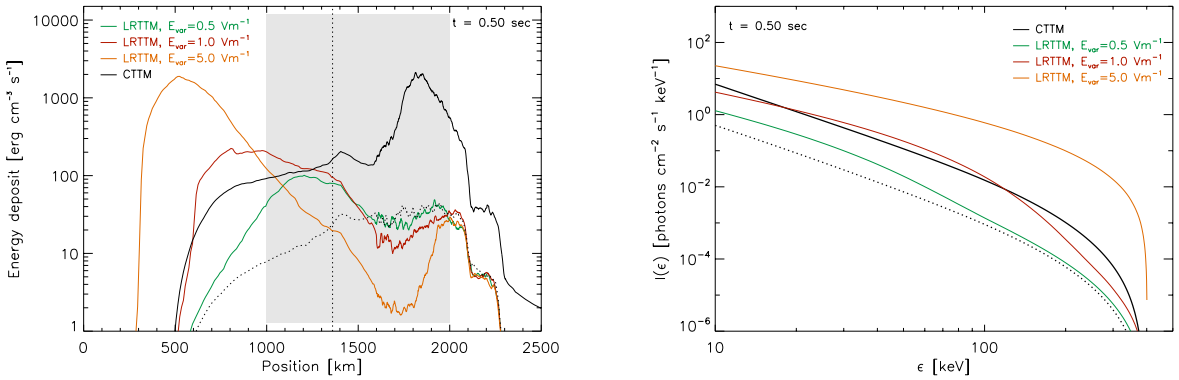

Figure 3. The energy deposits (left) and HXR spectra (right) at $t = 0.5$ s. The green, red and orange lines correspond to the LRTTM with the initial beam energy flux $\mathcal{F}_0 = 2.5 \times 10^9$ erg cm^{-2} s^{-1} and field variances $\mathrm{var}(E) = 0.5, 1$ and 5 V m^{-1}, respectively. The black lines indicate the energy deposits and HXR spectra for the CTTM, where the black solid and dotted lines correspond to the initial energy fluxes $\mathcal{F}_0 = 5 \times 10^{10}$ erg cm^{-2} s^{-1} and 2.5×10^9 erg cm^{-2} s^{-1}, respectively. The grey area indicates the secondary re-acceleration region, the vertical dotted line the bottom boundary of the magnetic mirror.

heights from 1000 km to 2000 km.

The HXR fluxes and spectra produced in the vicinity of loop foot-points are computed according to [1] using the semi-relativistic cross-section given by [16]. All the results are presented at time $t = 0.5$ s after the beam injection into the loop at its apex, when the model is close to a quasi-steady state.

3. Results

The distribution functions of non-thermal electrons for the CTTM and LRTTM are shown in left and right panel of Fig. 2, respectively. The electrons propagating from the loop apex towards the photosphere ($\mu \sim 1$) are coded with shades of red, the electrons with $\mu \sim 0$ are coded with shades of green and the electrons reflected by the magnetic mirror or backscattered ($\mu \sim -1$) are coded with shades of blue. For the CTTM case, it is evident that the majority of electrons arriving from the primary acceleration site (colour coded red to brown), into the higher density region between the upper chromosphere ($s \approx 2000$ km) and the bottom boundary of the magnetic mirror ($s = 1360$ km), quickly lose their energies and increase their pitch angles due to the Coulomb collisions and the effects of converging magnetic field. As a consequence a low energy tail is formed in the chromosphere above the bottom boundary of the magnetic mirror. The tail is dominated by particles of $\mu \sim 0$ and these particles either completely thermalise their kinetic energies or are reflected by the magnetic mirror back towards the second foot-point. Only few particles with higher energies penetrate behind the bottom boundary of the magnetic mirror.

The right panel of Fig. 2 shows the distribution function for the LRTTM. Two tails in the distribution function can be identified. A low energy tail corresponding to the tail identified in the distribution function for the CTTM, but less distinct, and a tail aiming towards high energies, spatially located within the re-acceleration region. This tail is formed by the particles re-accelerated by the stochastic electric fields. Another obvious effect of the stochastic fields is the enhancement of the number of backscattered electrons, particularly at higher energies. Comparing the corresponding energy deposits, it is apparent that the presence of the re-acceleration field substantially increases the energy deposit and shifts its maximum towards deeper layers.

The energy deposits for several variances of the stochastic field are shown in the left panel of Fig. 3. The model indicates that an increase of var(E) results in a dramatic increase of the energy deposit into the lower atmosphere and also the maxima of the energy deposits can be shifted to very deep layers (see the deposit for var(E) = 5 V m^{-1}). If the deposits are integrated over the chromosphere and photosphere we can conclude that the latter mentioned variance of stochastic field can increase the integrated deposit of almost one and half order in comparison with the deposit obtained using the CTTM and equal initial beam energy flux (dotted black line in the left panel of Fig. 3).

In flares the non-thermal electron distribution functions, the spatial position, and the extent of the energy deposits are influenced by the instantaneous state of the target flare atmosphere, in particular by the density profile of the chromosphere, which corresponds to the history of flare heating [14], [17], [18]. Due to the interaction of the low-energy electrons, which are predominant in the beam, with the evaporated flare plasma a shift of their penetration depth higher into the atmosphere can be expected. Similar effects would be also present using a static flare chromosphere (e.g. models F1 or F2 [19]).

The corresponding HXR spectra are shown in the right panel of Fig. 3. The HXR intensities and power-law indices are dependent on the values of var(E). With increasing variances $I_{10\,\mathrm{keV}}$ (the intensity at 10 keV) increases and the power-law indices harden. Comparing the intensity $I_{10\,\mathrm{keV}}$ for the LRTTM with var(E) = 5 V m^{-1} and for the CTTM with equal initial beam energy flux (dotted black line in the right panel of Fig. 3) we again obtain an increase in $I_{10\,\mathrm{keV}}$ of one and half order.

The HXR photon fluxes at various energies as a function of height above the photosphere for the CTTM and LRTTM are shown in Fig. 4. These profiles are used to calculate the HXR source heights and vertical sizes as the profile first and second moments, respectively. It is apparent that the placement and parameters of the magnetic mirror strongly influence the size and position of the CTTM HXR source. The results are shown in Fig. 5. The vertical sizes of

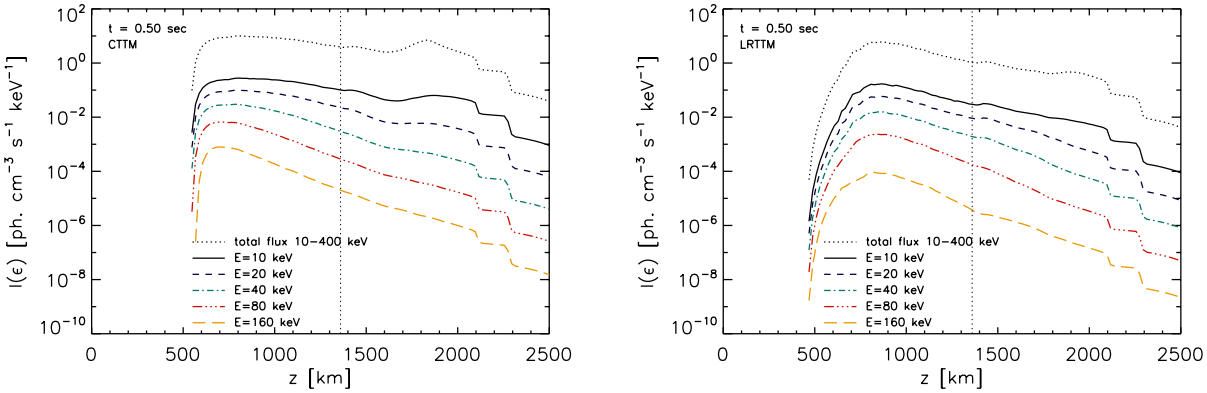

Figure 4. HXR photon flux emanating from the thick-target region as a function of height for selected photon energies (colour coded). Left for the CTTM, right for the LRTTM and $\mathrm{var}(E) = 1\ \mathrm{V\,m^{-1}}$. The dotted vertical line indicates the position of the bottom boundary of the magnetic mirror.

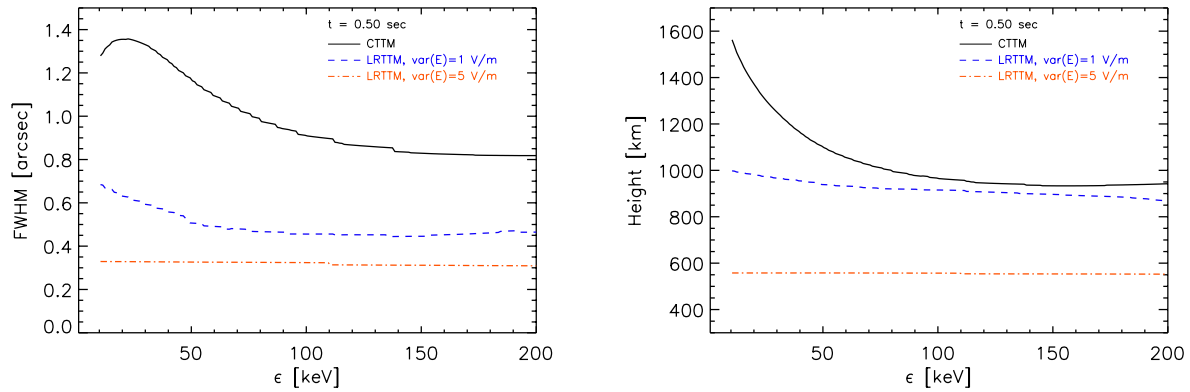

Figure 5. FWHM vertical sizes of the foot-point HXR sources (left panels) and the positions of the HXR emission maxima (right panels) versus photon energy for the CTTM (black solid lines) and the LRTTM (red dash-dotted lines) with $\mathrm{var}(E) = 1\ \mathrm{V\,m^{-1}}$ (upper panels) and $\mathrm{var}(E) = 5\ \mathrm{V\,m^{-1}}$ (lower panels).

HXR sources for the CTTM (left panel of Fig. 5 solid black lines) are about 1.2 arcsec for energies 10 – 30 keV. The source sizes decrease with increasing energy down to approximately 0.8 arcsec for energies above approximately 130 keV. For the LRTTM we found the HXR sources to be much more compact with increasing $\mathrm{var}(E)$ on all energies (compare dashed blue and dashed-dotted red lines in the left panel of Fig. 5) with a typical vertical source size 0.5 – 0.7 arcsec for $\mathrm{var}(E) = 1\ \mathrm{V\ m^{-1}}$ and approximately 0.3 arcsec for $\mathrm{var}(E) = 5\ \mathrm{V\ m^{-1}}$ on all energies.

Also the heights of the HXR emission maxima for the LRTTM are sensitive to the variance of stochastic field. With increasing $\mathrm{var}(E)$ the maxima tend to be placed deeper in the atmosphere (compare the blue dashed and red dash-dotted lines in the right panel of Fig. 5). The height of the HXR emission maximum for $\mathrm{var}(E) = 1\ \mathrm{V\ m^{-1}}$ is 1000 – 900 km for all energies. It corresponds to the height of the CTTM emission maximum for energies above 90 keV. The height for $\mathrm{var}(E) = 5\ \mathrm{V\ m^{-1}}$ is even only about 550 km for all energies and the source is thus much deeper than the CTTM source on all energies.

4. Conclusions

It has been shown that the presence of secondary re-acceleration in the region close to the flare loop foot-points reduces by one or one and half orders of magnitude (depending on the stochastic field parameters) the particle flux from the corona required to explain the observed HXR foot-point intensities. It also decreases the vertical size of the foot-point HXR sources. While the first findings agree with the results obtained by [3], [10], [11], the latter presents a problem.

Namely, the vertical sizes of HXR sources computed for the LRTTM are only 0.5 – 0.7 arcsec for $\mathrm{var}(E) = 1$ V m^{-1}, and even only 0.3 arcsec for $\mathrm{var}(E) = 5$ V m^{-1} on all energies. These values are much smaller than those obtained from the recent RHESSI observations (1.3 – 8 arcsec), see [9] and [8]. However, a comparison of the vertical sizes of X-ray sources for the LRTTM and CTTM models together with the multi-threaded chromosphere [20] offer a solution. Besides different densities in the multi-thread structure of the flaring chromosphere (which increases the vertical source size), in different threads a different distribution of the localised electric field can be expected; even with zero electric field (as in the case of the CTTM model). Therefore, integrating the vertical sizes of HXR sources for both considered models (LRTTM and CTTM) the observed vertical source sizes might be obtained. This suggestion will be tested in future models.

The heights of the HXR emission maxima for the LRTTM are in comparison with the CTTM substantially shifted towards the photosphere. The height above the photosphere, corresponding to height 0 km in the VAL C atmosphere model [12], decreases with the variance of the stochastic field. For $\mathrm{var}(E) = 5$ V m^{-1} we obtained the source height only approximately 550 km, which is not far from the heights of the white-light sources (305 ± 170 km and 195 ± 70 km) found from observations of white-light flares [21].

5. Acknowledgments

This work was supported by grants P209/10/1680 and P209/12/0103 of the Grant Agency of the Czech Republic. The research at the Astronomical Institute, ASČR leading to these results has received funding from the European Commission's Seventh Framework Programme (FP7) under the grant agreement SWIFT (project number 263340).

References

[1] Brown J C 1971 *Sol. Phys.* **18** 489
[2] Brown J C, Karlicky M, MacKinnon A L and van den Oord G H J 1990 *ApJS* **73** 343–348
[3] Brown J C, Turkmani R, Kontar E P, MacKinnon A L and Vlahos L 2009 *A&A* **508** 993–1000
[4] Sturrock P A 1968 A Model of Solar Flares *Structure and Development of Solar Active Regions* (*IAU Symposium* vol 35) ed Kiepenheuer K O p 471
[5] Kopp R A and Pneuman G W 1976 *Sol. Phys.* **50** 85–98
[6] Shibata K 1996 *Advances in Space Research* **17** 9
[7] Kontar E P and Brown J C 2006 *ApJ* **653** L149–L152 (*Preprint* `arXiv:astro-ph/0611170`)
[8] Battaglia M, Kontar E P, Fletcher L and MacKinnon A L 2012 *ApJ* **752** 4
[9] Battaglia M and Kontar E P 2011 *ApJ* **735** 42 (*Preprint* `1104.2997`)
[10] Turkmani R, Vlahos L, Galsgaard K, Cargill P J and Isliker H 2005 *ApJ* **620** L59
[11] Turkmani R, Cargill P J, Galsgaard K, Vlahos L and Isliker H 2006 *A&A* **449** 749–757
[12] Vernazza J E, Avrett E H and Loeser R 1981 *ApJS* **45** 635–725
[13] Varady M, Kašparová J, Moravec Z, Heinzel P and Karlický M 2010 *IEEE Transactions on Plasma Science* **38** 2249–2253
[14] Kašparová J, Varady M, Heinzel P, Karlický M and Moravec Z 2009 *A&A* **499** 923–934
[15] Varady M, Karlický M, Moravec Z and Kašparová J 2012 Influence of Static and Stochastic Electric Fields on Electron Beams Bombarding the Chromosphere *Fifth Hinode Science Meeting* (*Astronomical Society of the Pacific Conference Series* vol 456) ed Golub L, De Moortel I and Shimizu T p 203
[16] Haug E 1997 *A&A* **326** 417–418
[17] Abbett W P and Hawley S L 1999 *ApJ* **521** 906–919
[18] Allred J C, Hawley S L, Abbett W P and Carlsson M 2005 *ApJ* **630** 573–586

[19] Machado M E, Avrett E H, Vernazza J E and Noyes R W 1980 *ApJ* **242** 336–351
[20] Kontar E P, Hannah I G, Jeffrey N L S and Battaglia M 2010 *ApJ* **717** 250–256 (*Preprint* 1005.0599)
[21] Martínez Oliveros J C, Hudson H S, Hurford G J, Krucker S, Lin R P, Lindsey C, Couvidat S, Schou J and Thompson W T 2012 *ApJ* **753** L26 (*Preprint* 1206.0497)